Surface Rutilization of Anatase TiO_2 Nanorods for Creation of Synergistically Bridging and Fencing Electron Highways

Jiazang Chen,[1] Hong Bin Yang,[1] Hua Bing Tao,[1] Liping Zhang,[2] Jianwei Miao,[1] Hsin-Yi Wang,[1] Junze Chen,[2] Hua Zhang,[*,2] and Bin Liu[*,1]

[1] School of Chemical and Biomedical Engineering, Nanyang Technological University, 62 Nanyang Drive, Singapore 637459, Singapore, E-mail: liubin@ntu.edu.sg

[2] School of Materials Sciences and Engineering, Nanyang Technological University, 50 Nanyang Avenue, Singapore 639798, Singapore, E-mail: hzhang@ntu.edu.sg

Keywords: charge transport, charge transfer, surface rutilization, TiO_2 electrodes, photoelectrochemical cells

Abstract: In a photoelectrochemical cell, the most concerned issue in the nanostructured TiO_2 electrode is the charge transport, which consists of the internal movement of electrons in TiO_2 nanostructures and the inter-grain charge transfer. Here, inspired by electrochemical studies on different polymorphs of TiO_2, we propose to bridge the adjacent building blocks and fence the electron transport highways in TiO_2 electrodes by surface rutilization of anatase nanorods. The ultrathin rutilized layer completely coated on the anatase surface has a slightly higher conduction band edge than that of anatase. The obtained surface rutilized anatase nanorods can not only improve the inter-grain charge transfer while maintaining fast electron transport within anatase, but also minimize the internal energy consumption and protect the electrons in TiO_2 electrodes from recombination, which are beneficial to the charge collection and can significantly improve the photovoltaic performance of photoelectrochemical cells.

1. Introduction

As known, TiO_2 is the most widely used semiconductor material in photoelectrochemical (PEC) applications owing to its unique electrical and optical characteristics which could offer superior performances in photovoltaic devices, water splitting cells, and so on.[1] Rutile and anatase are the most common phases of TiO_2. Although the anatase TiO_2-based PEC systems usually exhibit better performance compared to the rutile TiO_2, the emerging of the synergistic effect between these two polymorphs becomes a promising pathway to design more efficient electrodes/catalysts.[2]

Despite the intensive studies, there is no generally accepted experimental evidence to clarify the intrinsic difference related to PEC behaviors between these two polymorphs.[3] Explanations for the observation that anatase is superior to rutile in PEC cells are mainly based on the theoretically higher charge mobility and longer excited-state lifetime of anatase.[4] Moreover, the band alignment between anatase and rutile used to explain their synergistic effect is also under controversy.[5] The lack of credible proof to discriminate the intrinsic differences between these two polymorphs becomes a bottleneck to design efficient TiO_2 electrodes/catalysts to take good use of the synergistic effect.

In the PEC application, TiO_2 electrodes are usually made of nanostructures.[1a, 6] In this situation, it is not rational to apply the physical parameters obtained from the bulk crystalline materials to explain the phenomena in PEC systems, in which the electronic processes and band structures of the semiconductors are sensitively affected by certain factors, such as the ingredient of electrolyte, the density of (photo)-electrochemically doped electrons, and in particular the construction of electrodes.[6-7] For example, due to grain boundary scattering, the charge mobility in field-free electrodes is usually three orders of magnitude smaller than that in bulk crystals.[8] In this case, the boundary scattering plays a crucial role in charge mobility.[8d, 8e] Therefore, the transport of charges

in mesoporous electrodes will be no longer solely predominated by the *internal charge movement*, since the *inter-grain charge transfer* also plays a profound role in the charge diffusion. Furthermore, the electronic processes occurred in PEC cells are rather environment dependent. Since the physical methods like X-ray photoemission and Hall Effect techniques for the TiO_2 test are carried out under *dry ambient conditions*, certain factors like band edge movement and charge depletion are ignored. In addition, in certain electrochemical and/or PEC systems like photovoltaic devices, the charge recombination usually reflects the transfer of extrinsically given electrons from the semiconductor to the electron acceptors (oxidized species) in the electrolyte, rather than the annihilation of the pairs of intrinsic positive and negative charges in the excited states.[9] Therefore, the application of parameters obtained from boundary-less bulk crystals using *dry physical methods* to explain the better performance of anatase TiO_2-based PEC cells is somehow intuitive and result-oriented, which cannot give us satisfied elucidation, nor provide valuable information to consciously utilize the synergistic effect.

Here, based on the electrochemical study on the difference between rutile and anatase TiO_2 in PEC systems, we propose to rutilize the surface of anatase TiO_2 nanostructures to reduce the energy consumption during the electronic processes and save the charge from recombination. We first investigate the polymorph differences by comparing the parameters of electronic processes occurred in porous TiO_2 electrodes made of these two polymorphs. To eliminate the interference of architectural effect and obtain reliable parameters, we manage to make the shape and size of the nanostructures, as well as the construction of TiO_2 electrodes made of different polymorph the same. The promising band alignment between these two polymorphs and the efficient inter-grain charge transfer offered by the participation of rutile phase maps the synergistic effect occurred in the electrodes made of surface rutilized anatase TiO_2. The ultrathin rutile layer, which is *in situ*

transformed from the anatase phase and completely covers the surface of anatase nanostructures, can efficiently improve the inter-grain electronic connectivity by bridging the adjacent building blocks and protect the charge in the semiconductor from recombination on semiconductor-electrolyte interface (SEI) by fencing the electron transport highways in TiO_2 electrodes.

2. Results and discussion

2.1. Preparation of Anatase and Rutile TiO_2 Nanorods with Similar Size and Morphology. For nanostructured semiconductor electrodes, the electronic processes, especially the transport of charge, are strongly architecture-dependent. Some of their features, including porosity of semiconductor films, morphology of building blocks, and coordination number and necking area between grains in the semiconductor electrodes can profoundly influence their electronic processes.[8d, 8f, 10] Among these features, the shape and size of the building blocks are intrinsic. Therefore, in order to obtain reliable parameters for further comparing the difference in the electronic processes occurred in semiconductor electrodes, the preparation of TiO_2 nanostructures of different polymorphs with similar shape and size becomes the prerequisite. Generally, rutile tends to grow into one-dimensional (1D) rod-like nanostructures while the preferred shape for anatase is particulate in hydrothermal systems. Recently, the development of thermodynamically driven 1D evolution of anatase inspires us to further explore the synthetic strategy to grow anatase TiO_2 nanostructures with similar shape and size to the rutile counterparts.[10b]

During the hydrothermal growth of anatase TiO_2 nanorods, morphological features including length, diameter, and aspect ratio increase with the ammonia concentration (Figure S1).[10b] For the rutile counterparts, the features including the aspect ratio are mainly controlled by the kinetics of the linear assembly of six-fold coordinated hydrolyzed monomers by sharing opposite edges in the

equatorial of octahedrons.[11] The morphologies of the rutile nanostructures can be tuned by modifying the acidity in reaction and changing the titanium precursors (Figure S2). Therefore, TiO_2 nanostructures with similar shape and size for these two polymorphs can be obtained by co-adjusting the experimental parameters (see the Method Section for details) (Figure 1, Figure S3, and Figure S4).

The anatase and rutile TiO_2 nanostructures used for investigation of their electrochemical behaviors were characterized by field emission scanning electron microscopy (FESEM) and transmission electron microscopy (TEM). The anatase and rutile TiO_2 nanostructures synthesized by hydrothermal treatment of titanium precursors in alkaline and acidic solutions have very similar shape and size. The FESEM images (Figure 1a) and X-ray diffraction (XRD) patterns (Figure S3) show that the TiO_2 nanostructures synthesized by hydrothermal treatment of titanium isopropoxide in alcoholic ammonia water system are of rod-like shape and phase-pure anatase with an average diameter of ~40 nm and length of ~120 nm. TEM image (Figure 1b) and selected area electron diffraction (SAED) patterns (Figure 1c) further confirmed that the nanorods are single-crystalline anatase and have a distorted quadrilateral shape in the tip. The angles in the tip are 137^o and 112^o, which can be attributed to the angles between (101) and (-101) planes, and between (101)/(-101) and (002) planes of anatase crystals, respectively (Figure 1b, c). The rutile TiO_2 nanostructures (Figure 1d, e) prepared by hydrothermal treatment of $TiCl_4$ solution have very similar morphology to that of anatase counterparts (Figure 1a, b). Moreover, the SAED (Figure 1f) and XRD patterns (Figure S3) prove that the rutile TiO_2 nanostructures are phase-pure single-crystalline.

2.2. Electrochemical Investigation of Intrinsic Polymorph Differences. 2.2.1. Determination of Trap-Free Diffusion Coefficients. To illustrate the intrinsic difference between the anatase and rutile TiO_2 nanostructure, the electronic processes occurred in the electrodes made of them were

investigated by electrochemical impedance spectroscopy. For cells with good carrier collection efficiency, the electron transport in TiO_2 films appears as the Warburg-like diffusion behavior in the high-frequency range and the interfacial charge recombination process grows into a large semicircle in the low-frequency region (Figure S5).[12] The electronic processes in PEC cells are well described by the transmission line model (Figure S6).[12-13] By fitting the obtained impedance spectra with the transmission line model,[12-13] we obtained the parameters including electron transport resistance (R_t), interfacial charge recombination resistance (R_{ct}), and chemical capacitance (C_μ) that describe the electronic processes in the semiconductor electrodes.

The propagation of electrons in nanostructured semiconductor electrodes is mainly driven by diffusion, because of the effective electrolyte shielding of space charge.[14] The diffusion coefficient of the electrons within the mesoporous semiconductor electrodes strongly depends on the structural architectures and the density and distribution of the trap states located in the band gap:

$$D_n = \frac{1}{1+\frac{\partial n_L}{\partial n_C}} D_0 \tag{1a}$$

where n_L is the trapped electron density, n_C is the conduction band electron density. When the electronic Fermi level (E_F) is far away from the conduction band edge (E_{CB}), namely $E_F < E_{CB} - k_B T$ (here k_B is the Boltzmann constant and T is the tempetature), the term $\partial n_C / \partial n_L$ is small, and then the eqn. 1a becomes:

$$D_n = \left(\frac{\partial n_C}{\partial n_L}\right) D_0 \tag{1b}$$

The pre-factor $\partial n_C / \partial n_L$ reflects the delay of the response of chemical diffusion coefficient by the trapping and detrapping processes. It is therefore elicited that the effective electron diffusion coefficient (D_n) is governed by the density of localized states and the depth of the trap sites. Under quasi steady-state condition, the effective diffusion coefficient of electrons in TiO_2 electrode can be

obtained by using small perturbation techniques, such as intensity modulated photocurrent spectroscopy (IMPS) and impedance spectroscopy. Here we calculated D_n from the transport resistance (R_t) and chemical capacitance (C_μ) based on $D_n = (R_t C_\mu)^{-1}$. D_0 is the constant diffusion coefficient of freely mobile electrons (trap-free charge transport) at or above the transport edge of the semiconductor mesoporous electrodes, which is closely related to the structural architectures and intrinsic property of the semiconductor.[8d] Therefore, the value of D_0 would be a characteristic parameter for a given semiconductor electrode, which provides constructional features, including porosity of semiconductor films, morphology of building blocks, and coordination number and necking area between grains.[8d, 8f, 10] The chemical diffusion coefficient can be obtained from:

$$D_n = \frac{N_C T_0}{N_L T} \cdot \exp\left[\left(E_F - E_C\right) \cdot \left(\frac{1}{k_B T} - \frac{1}{k_B T_0} \right) \right] D_0 \qquad (1c)$$

where N_C is the effective density of states in the conduction band, N_L is the total density of the localized states, k_B is the Boltzmann constant, and T_0 is the characteristic temperature which determines the depth and distribution of trap sites below the lower edge of the conduction band. When $E_F \approx E_{CB} - k_B T$, the term $\partial n_C / \partial n_L \geq 1$, the chemical diffusion coefficient of charge is equal to the constant diffusion coefficient ($D_n \approx D_0$, according to eqn. 1a). Therefore, the constant diffusion coefficient can be estimated by extrapolating the relationship of D_n–E_F obtained at various temperatures.[8d]

Figure 2 shows the exponential variation of D_n values over the electronic Fermi level at various temperatures. As shown by the D_n–E_F relationship, the electrodes made of rutile and anatase TiO_2 nanostructures with similar architectures (Figure 1, and Figure S7) exhibit very similar values of trap-free diffusion coefficients. The D_0 values for rutile and anatase TiO_2 electrodes are 0.0104 and 0.0147 cm^2/s, respectively, corresponding to 0.402 and 0.568 cm^2/Vs for electron mobility at room temperature. Taking into account of the size of our TiO_2 nanostructures, these values of trap-free

diffusion coefficient and the related mobility are rational as compared with the reported parameters.[8d, 10b]

2.2.2. Band Alignment and Electronic Processes. It has been established that the conductivity of electrons in TiO_2 network is exclusively dependent on the number of free electrons in extended states:[15]

$$\sigma = q\mu n \tag{2a}$$

where q is the elementary charge, μ is the mobility, and n is the density of free electrons. For diffusion of charged particles like electrons, the mobility equation can be described as:

$$\mu = \frac{qD_0}{k_B T} \tag{2b}$$

Although these electrodes are made of different TiO_2 materials, they would have similar values of conductivity if densities of electrons in the conduction band are kept the same. Therefore, the electronic conductivity can provide a reference for the position of the E_F with respect to the E_{CB}:[15-16]

$$\sigma = \sigma_0 \exp\left[-\frac{(E_{CB} - E_F)}{k_B T}\right] \tag{2c}$$

where σ_0 is a constant related to charge mobility. The electronic conductivity is independent of number of traps, because it is only related to the steady-state transport and reflects the rate of displacement in the transport band.[17] In contrast, the electron diffusion coefficient of semiconductor network is strongly dependent on the occupation of traps.[14] Thus, it is reasonable to take the electron conductivity as a parameter to compare the electrochemical properties of different semiconductor electrodes at the same electron density. The conductivity of TiO_2 network can be calculated from R_t by using the geometrical parameters.

In the redox couple-based PEC and electrochemical cells, e.g., the very exemplificative cells based

on I^-/I_3^- couples, the redox potential (E_{redox}) is stationary. The bias potential of the cell is related to the difference between the electronic Fermi level in the TiO_2 and E_{redox}. Therefore, the relationship of potential-conductivity can provide the difference between the E_{CB} of TiO_2 and E_{redox}:

$$\sigma = \sigma_0 \exp\left[\frac{q}{k_B T}\left(V + \frac{E_{Redox} - E_{CB}}{q}\right)\right] \quad (2d)$$

Figure 3a gives the comparison of potential-dependent conductivity of the cells assembled from anatase and rutile TiO_2. Under the similar biased potential (electronic Fermi level), the conductivity of rutile electrode is much smaller than that of anatase. Since the mobility of charges in the two electrodes is similar, the rather high charge transport resistance suggests that the density of free electrons in the rutile electrode is low, as compared to the anatase electrode. According to the eqns. 2a-d, the lower density of free electrons suggests that the position of conduction band edge for rutile TiO_2 is higher than that of anatase TiO_2 (Figure 3).

Chemical capacitance is proportional to the density of electronic states (DOS) in the band gap of semiconductor. Figure 3b shows the relationship between chemical capacitance and electrode potential for both the anatase and rutile TiO_2 electrodes. It can be seen that all data points in both of two plots lie in almost the same line and have similar slopes over the measured potential range, indicating that the density and distribution characteristic of band tail states below the electronic Fermi level for the anatase and rutile TiO_2 electrodes are very similar (Figure 3b, c). Despite the similar electronic states below the electronic Fermi level, the density of trap sites below the conduction band is higher for the rutile electrode (Figure 3c), as compared to that of the anatase electrode. Therefore, the effect of trapping/detrapping events on the charge transport would be more obvious for the rutile electrode.

Our aforementioned inference is rational. The construction features like the porosity of electrodes and the cells used for studying the electronic structures are similar to the widely applied

electrochemical and PEC systems, suggesting that our result is of more extensive universality. Besides, our proposed band alignment is in good agreement with the results obtained by Scanlon *et al*[5b] and Klein *et al*,[18] who determined the difference of band position for the two polymorphs of TiO_2 by combination of the material simulation techniques and X-ray photoemission experiments.

2.2.3. Effect of Trap States on Charge Transport. The distribution of trap states below the conduction band will prolong the charge transport time, according to the multiple trapping (MT) model.[19] In this situation, D_n grows exponentially as E_F shifts towards more negative potential (Figure S8). For the rutile TiO_2 electrode, the density of trap states below the conduction band is relatively high, as compared to the anatase electrode (Figure 3b, c). Therefore, the rutile electrode shows a smaller electron diffusion coefficient (Figure S8, and Figure 4). Besides, the trap states located at/near the surface of the semiconductor will act as intermediates to trap electrons and increase the probability of charge recombination.[20] The relatively higher density of trap states in the rutile TiO_2 electrode will aggravate the interfacial leakage of charges on the SEI (Figure S9). By virtue of these benefits like the retarding of interfacial charge recombination for the cells with anatase TiO_2 electrodes, the lifetime (τ_n) and the diffusion length (L_n) of electrons in the semiconductor electrodes can be effectively increased (Figure S10).

Moreover, due to the larger coefficient for charge diffusion and much longer surviving time for the electrons in the anatase electrodes as well as the ability to travel longer distances (Figure 2, Figure 4, Figure S8, and Figure S10), PEC systems made of anatase electrodes exhibited better charge collection performance. In our photovoltaic devices, i.e., dye-sensitized solar cells (DSSCs), the photocurrent-voltage characteristics (Figure S11) shows that the cell assembled from the rutile TiO_2 electrode gave the short-circuit photocurrent density (J_{SC}) of 10.06 mA/cm^2, open-circuit voltage (V_{OC}) of 773 mV, fill factor (*FF*) of 0.760, and energy conversion efficiency (η) of 5.91%. By

replacing the rutile TiO_2 electrode with anatase TiO_2 electrode, the values for J_{SC}, V_{OC}, and *FF* increase to 14.93 mA/cm^2, 783 mV, and 0.763, respectively, with energy conversion efficiency of 8.92%. Although the conduction band edge of anatase TiO_2 is ~100 mV lower (Figure 3a, c) than that of rutile polymorph, the open-circuit voltages for the two cells (anatase and rutile TiO_2) are similar. Analogous result has also been reported by Frank *et al*,[21] who proposed that the semiconductor electrodes with lower conduction band edge could offer relatively higher voltage by blocking the interfacial charge leakage. Here in our case, the effective suppression of interfacial charge recombination (Figure 4, and Figure S9) can increase the density of electrons in the anatase TiO_2 electrode and further upshift the electronic Fermi level.

2.3. Bridging and Fencing Electron Highways in Nanostructured Electrodes. 2.3.1. Investigation of Inter-Grain Charge Transfer by Deconvolution of Charge Mobility. It is generally accepted that the charge mobility in crystalline anatase TiO_2 is larger than that in rutile counterpart.[22] For example, the electron mobility in the single-crystalline anatase TiO_2 can reach as high as 10-20 cm^2 V^{-1}s^{-1}, while for the single-crystalline rutile TiO_2, it decreases to 0.1-1 cm^2 V^{-1}s^{-1}. However, the situation is rather different in the porous nanostructured semiconductor electrode. It has been reported that the value of D_0 in nanostructured anatase TiO_2 films is only in the range of 10^{-3} - 10^{-2} cm^2 s^{-1}, corresponding to a charge mobility of ~0.003 - 0.03 cm^2 V^{-1}s^{-1}, which is ~3 orders of magnitudes less than that in the single-crystalline materials, most likely arising from the *inter-grain scattering*.[8] Since the charge transport takes place in both the interior (*internal electron movement*) of the building blocks and the grain boundaries (*inter-grain charge transfer*), it can be modeled as being connected in series and the trap-free diffusion coefficient in nanostructured electrodes (or the mobility) can be expressed as:

$$\frac{1}{D_0} = \frac{1}{D_{0,\text{in}}} + \frac{1}{D_{0,\text{ex}}} \tag{3a}$$

where $D_{0,in}$ and $D_{0,ex}$ are trap-free diffusion coefficients of charges in the interior of the semiconductor and across grain boundaries, respectively. Therefore, the mobility of charges (μ) in each element can be described as:

$$\frac{1}{\mu} = \frac{1}{\mu_{in}} + \frac{1}{\mu_{ex}} \tag{3b}$$

where μ_{in} and μ_{ex} describe the charge mobility in the interior of the semiconductor and across grain boundaries, respectively. In our system, the similar D_0 value for the two electrodes (anatase and rutile TiO_2, Figure 2) can be interpreted as the following: although the electron mobility in the interior of rutile crystal is smaller than that in the anatase counterpart ($D_{0,in,rutile} < D_{0,in,anatase}$), the more efficient inter-grain charge transfer ($D_{0,ex,rutile} > D_{0,ex,anatase}$) can compensate for the shortage of intrinsic internal charge movement and bring the total charge mobility in the rutile electrode up to the similar value as the anatase electrode. To further verify our assumption, we investigated the effect of inter-grain necking conditions on the transport of charges in TiO_2 electrodes. In order to obtain the insightful information on the impact of necking condition (related to $D_{0,ex}$) while keeping the internal charge movement ($D_{0,in}$) unchanged, we managed to change the features of necking area and coordination number by changing the porosity of the TiO_2 electrodes. By plotting the trap-free diffusion parameters over the porosity (Figure 5a), it can be seen that the influence of porosity on D_0 is much more significant for the anatase electrode. The sensitive variation of D_0 over the porosity suggests that in anatase electrode, the inter-grain charge transfer plays a more predominant role on charge transport than the rutile counterpart. Associated with the fact of faster internal electron movement in the anatase TiO_2[22] and the similar value of D_0 for the anatase and rutile TiO_2 electrodes (Figure 2), it is expected that the inter-grain charge transfer will be more efficient in the rutile electrode.

2.3.2. Improvement of Charge Mobility by Composition. Since the shape and size for both of the

rutile and anatase TiO_2 nanostructures are similar, and the technique parameters (e.g., solid concentration of TiO_2 in the paste, ramping temperature, heating duration at the desired temperature, and cooling) used for the fabrication of porous electrodes are the same, it is expected that the architectural features of resultant films would be identical. Our anticipation was further verified by the nitrogen adsorption-desorption and dye desorption measurements, which showed that the semiconductor electrodes made of these two polymorphs of TiO_2 nanostructures have similar pore distributions and surface area for dye loading (Figure S7). The similar trap-free diffusion coefficient and mobility of charges (Figure 2) in the electrodes made of rutile and anatase TiO_2 are most likely resulted from the more efficient inter-grain charge transfer between building blocks in the rutile electrodes. By introducing rutile TiO_2 into anatase nanostructured electrodes, the better inter-grain connectivity can help to improve the charge transfer between the building blocks made of these two polymorphs. Therefore, the anatase building blocks in the mesoporous electrodes can be bridged by the rutile nanostructures. This conclusion is further verified by the fact that the mobility of electrons is improved in the electrodes made of mixed phases of rutile and anatase (Figure 5b). Although the position of conduction band edge of rutile TiO_2 is slightly higher than that of anatase TiO_2, which makes the electrons in the phase-mixed electrodes consume additional energy to overcome the barriers during the charge transport, the benefit resulted from the promotion of inter-grain connectivity in phase-mixed electrodes is obviously greater than those unfavorable energy dissipations.

The higher value of trap-free diffusion coefficient is beneficial for the charge transport when the concentration of charges in the semiconductor electrodes is high. However, the situation is not always delightful.[8d] According to the MT model, lowering the concentration of photo-induced charge carriers rapidly decreases the charge diffusion coefficient. For a semiconductor electrode

with higher density of trap states in the band gap, it requires much more free electrons to keep a desired charge diffusion coefficient. As a result, a semiconductor electrode with high charge mobility still exhibits the relatively low charge diffusion coefficient if the concentration of charge carriers in it is not high enough.[8d, 8f] In our system, when the concentration of photo-induced charge carriers is high, the improved inter-grain connectivity benefited from the introduction of the rutile building blocks can facilitate the transport of charges in the electrode made of phase-mixed TiO_2 (90% anatase and 10% rutile) (Figure S12). However, the charge diffusion rate decreases rapidly as the illumination intensity goes down. The charge diffusion coefficient of the phase-mixed TiO_2 electrode becomes even smaller than that of pure anatase electrode at low concentration of photogenerated charge carriers (Figure S12). Since the photogenerated electrons have to pass the rutile building blocks in the phase-mixed electrodes before they reach the conducting substrate, the higher density of trap states in rutile building blocks will increase the probability of trapping/detrapping events, resulting undesirably in decrease of charge diffusion coefficient. This will also decrease the charge collection efficiency and thus the performances of the photovoltaic devices made of these electrodes (Figure S13).

2.3.3. Bridging and Fencing Electron Highways by Surface Rutilization. In order to alleviate the trapping/detrapping events while fully exerting the benefit of improved inter-grain connectivity, it is desired to reduce the travel distance of electrons in the rutile building blocks. To achieve this goal, formation of thin rutile layers between the adjacent anatase building blocks should be beneficial. Toward this end, we developed a facile surface rutilization method to *in situ* form a homogeneous thin rutile layer on anatase nanostructures to minimize the internal energy dissipation. Surface rutilization of anatase TiO_2 was realized by hydrothermal treatment of anatase nanostructures in HCl solution (Figure 6a, b, and Figure S14). Features, including crystallinity and thickness of

rutilized thin layer could be adjusted by changing the reaction time and temperature (Figure S14). With the rutilized surface, the inter-grain charge transfer between adjacent anatase building blocks can be bridged in the nanostructured TiO_2 electrodes. As determined by impedance spectroscopy, the trap-free diffusion coefficient of electrons in this kind of electrodes reaches as high as 0.148 cm^2/s (Figure 6c), which is about 10 time higher than that obtained in the pure anatase TiO_2 electrode (0.0147 cm^2/s, Figure 2). Besides, because of the promising band alignment, the isolation of exposed anatase phase to the electrolyte by the formed rutilized thin layers can effectively retard the electrons in the nanostructured electrodes from recombination with oxidized species on the SEI (Figure S15), which can further improve the charge collection efficiency (Figure S16). Since the rutile layer is ultrathin (~1-4 nm, Figure 6, Figure S12, and Figure S17), the significant reduction of electron travel distance in the interior of rutile TiO_2 can accelerate the total charge diffusion. Besides, the relatively lower probability of trapping/detrapping events in the electrodes based on surface rutilized anatase TiO_2 nanostructures can further improve the charge transport even at low density of photogenerated electrons (Figure S12).

Our strategy is rather different from the case of commonly adopted $TiCl_4$ post-treated TiO_2 electrodes in DSSCs. The main purpose for heterogeneous $TiCl_4$ post-treatment is to form TiO_2 coatings on the electrode surface, which would be beneficial to the charge collection by blocking the interfacial charge transfer.[23] From the viewpoint of electrode configuration, the $TiCl_4$ post-treatment only forms thin TiO_2 coatings on the *exposed* surface of the porous electrodes (Figure 6a), rather than fully coat the surface of the building blocks. Therefore, the improvement in the inter-grain charge transfer would be tiny, due to the absence of the bridging rutilized thin layer between adjacent anatase building blocks. As estimated from the temperature-dependent D_n, the trap-free diffusion coefficient of electrons in the $TiCl_4$ post-treated TiO_2 electrode is 0.0175 cm^2/s

(Figure S18), which is quite similar to that of the untreated electrode (0.0147 cm^2/s, Figure 2). In our case, the anatase nanostructures were completely coated by the rutilized surface thin layers prior to fabricate the electrodes, which are quite similar to the anatase@rutile core-shell structures. Therefore, in the formed electrodes, the connectivity between adjacent anatase building blocks can be significantly improved by the bridging rutilized thin layer, which can facilitate the inter-grain charge transfer (Figure 6).

By virtue of these merits, the PEC devices fabricated by this kind of TiO_2 electrodes exhibit better performance. Our hypothesis was well supported by the photovoltaic characteristics of the DSSCs assembled from these TiO_2 materials (Figure S19). The photocurrent-voltage characteristics show that J_{SC} and the energy conversion efficiency for the cell made of surface rutilized anatase TiO_2 electrode are 16.65 mA/cm^2 and 9.62 %, respectively, which are much higher than those for the cell with plain anatase nanostructures (Figure S11).

3. Conclusion

We have demonstrated that in nanostructured TiO_2 electrodes, the internal movement of electrons is faster inside anatase building blocks, while the rutile counterparts exhibit more efficient inter-grain charge transfer. As a result, introduction of rutile into the TiO_2 electrodes can improve the charge mobility by facilitating the inter-grain charge transfer between the adjacent building blocks, although the conduction band edge of rutile TiO_2 as we observed is slightly higher than that of anatase polymorph. To reduce the energy dissipation by the trapping/detrapping events in rutile TiO_2 and improve the charge collection by retarding the interfacial charge recombination, simultaneously bridging the inter-grain charge transfer and fencing electron highways in nanostructured anatase TiO_2 electrodes are realized by using the surface rutilized anatase nanostructures as the building blocks. The significance of this work lies in the successful

demonstration of redox couple based photoelectrochemical cells. Furthermore, we believe that our work can also prompt the sequential development of solar water splitting cells, perovskite solar cells, energy storage devices, and other relevant applications.

4. Experimental Section

4.1. Preparation of TiO_2 materials. Anatase TiO_2 nanorods were synthesized based on our previously reported method with slight modification.[10b] Briefly, 3.2 g of NH_4Cl (Merck) were firstly dissolved in 32 mL of isopropanol (Pr^iOH, Fisher Scientific, assay: > 99.5%, water: < 0.2%) in a Teflon-lined stainless steel autoclave (100 mL). The mixture was stirred at ambient condition for 5 min before addition of 2 mL of titanium (IV) tetraisopropoxide (TTIP, Sigma-Aldrich, 97%). After stirring for 30 min, 40 mL of (diluted) ammonia water was added. To tune the aspect ratios of the anatase nanorods, the (diluted) ammonia water with various concentrations was used. The volume ratios of commercially available ammonia water (28-30%) to the diluting water were 0 : 1, 1 : 4, 2 : 3, and 1 : 0. After stirring for another 5 min, the autoclave was sealed and kept at 170 ºC for 72 h, and the resulting precipitates were collected and washed with deionized water for three times and then ethanol for three times. The rutile TiO_2 nanorods were synthesized by one-step hydrothermal treatment of $TiCl_4$ solution. Briefly, 15 mL of $TiCl_4$ solution (2.5 M, Merck) were added into 60 mL of water in a 200 mL flask under stirring. The obtained clear solution was then heated to 90 ºC and kept for 2 h. After that, the slurry was transferred into a sealed Teflon-lined autoclave which was heated at 160 ºC for 12 h to grow rutile TiO_2 nanorods. Surface rutilization of anatase TiO_2 nanorods was realized by hydrothermal treatment of the anatase TiO_2 nanorods in HCl solution (6M) at 180-200 ºC for 24-72 h.

4.2. Fabrication of Sandwich-Type Cells. The TiO_2 paste with rutile or anatase nanorods was prepared by ultrasonically dispersing the TiO_2 nanostructures in the mixture of water and ethanol

(v:v = 1:1). After sonication, the solid was collected by centrifugation and dried overnight under vacuum at 90 ºC. The TiO_2 paste was prepared by dispersing the dried nanostructures (450 mg) into 2.5 mL of terpineol (Sigma-Aldrich) under stirring. Prior to addition of the dried TiO_2 powders, certain amount (typically 225 mg) of ethyl cellulose (Sigma-Aldrich) was dissolved into the terpineol to tune the viscosity of the paste and the porosity of the final sintered TiO_2 films. The TiO_2 paste was then deposited on fluorine-doped tin oxide conducting glass substrate (FTO, 14 Ω/square, Nippon Sheet Glass) by screen printing (Safer, Polyester, 250 meshes). Then the film was heated to 500 ºC at rate of 15 ºC/min and kept for 30 min. After cooling down to 80 ºC, the TiO_2 electrode was immersed overnight in an N719 dye (Dyesol) solution (0.5 mM). The electrode was then rinsed with acetonitrile and dried. Subsequently, the sensitized TiO_2 film was assembled with a platinized FTO glass into sealed sandwich-type cell by heating with a Surlyn film (60 μm in thickness). After that, one drop of electrolyte was filled into the inter-electrode space by vacuum injection. The electrolyte was composed of 0.1 M of lithium iodide (LiI, Sigma-Aldrich), 0.6 M of tetrabutylammonium iodide (TBAI, Sigma-Aldrich), 0.05 M of iodine (I_2, Sigma-Aldrich), and 0.5 M of 4-*tert*-butylpyridine (*t*BP, Sigma-Aldrich) in acetonitrile.

4.3. Electrochemistry and Photoelectrochemistry. The electronic processes occurring in the semiconductor electrodes were mainly characterized by impedance spectroscopy, which was performed with a computer controlled Solartron potentiostat with a frequency range of 500k-0.05 Hz. The amplitude of the ac signal was 10 mV. The obtained spectra were fitted with Z-view software. Electron transport resistance (R_t), interfacial charge recombination resistance (R_{ct}), and chemical capacitance (C_μ) can be obtained from the fitting results. The electronic conductivity (σ) of TiO_2 network can be calculated from R_t by using the geometrical parameters. And the electronic process features, such as lifetime (τ_n), diffusion coefficient (D_n), and diffusion length (L_n) of

electrons in the semiconductor electrode can be calculated by the following equations:

$$\tau_n = R_{ct} C_\mu \tag{4}$$

$$D_n = \frac{1}{R_t C_\mu} = \frac{\sigma}{C_\mu} \tag{5}$$

$$L_n = \sqrt{\sigma R_{ct}} = \sqrt{D_n \tau_n} \tag{6}$$

Determination of electron diffusion coefficient at various illumination intensities was carried out by stepped light-induced transient measurement of photocurrents.[24] The time constant was obtained by fitting the decay of the photocurrent transient to the function of $\exp(-t/\tau_c)$, where t is time and τ_c is the time constant for electron collection. The values of D_n can be obtained using the following equation:

$$D_n = d^2 / (2.35 * \tau_c) \tag{7}$$

where d is the thickness of the semiconductor film. The retarding of interfacial charge recombination by the rutilized surface was also determined by open-circuit voltage decay (OCVD) spectroscopy, which monitored the variation of electrode potentials over the time. The time constant (τ_n) for charge recombination can be obtained from the following equation:[25]

$$\tau_n = -\frac{k_B T}{q} \left(\frac{dV_{OC}}{dt} \right)^{-1} \tag{8}$$

where k_B is the Boltzmann constant, T is the tempetature, q is the elementary charge. The photovoltaic behaviors of the sandwich-type cells were characterized by recording the photocurrent-voltage (J-V) curves under A.M. 1.5 G illumination (100 mW/cm^2). The illumination was provided from an ABET solar simulator.

4.4. Materials Characterization. The TiO_2 nanostructures were characterized by X-ray diffraction (XRD) using a Bruker D8 X-ray powder diffractometer. Transmission electron microscopy (TEM) and high-resolution TEM (HRTEM) investigations were taken with a JEOL JEM-2010 field

emission electron microscope operated at 200 kV. The selected area electron diffraction (SAED) patterns of samples were obtained by the Fast Fourier Transform of the HRTEM image using DigitalMicrograph software (Gatan). Morphology of the samples was characterized by field emission scanning electron microscopy (FESEM) on a JEOL JSM-6701F electron microscope. Porosity of the TiO_2 was measured using nitrogen adsorption/desorption method on Quantachrome Autosorb-6 (AS6). The amount of dye uptake on the semiconductor electrodes was measured by dye desorption in ethanolic solution containing 0.1 M NaOH. The absorbance of the resulting solution was measured by UV-visible spectrophotometry (Varian Cary 4000).

Acknowledgements. This work was supported by Nanyang Technological University (M4080977.120.50000), Ministry of Education of Singapore (M4011021.120) under Academic Research Fund (AcRF) Tier 2 (ARC 26/13, no. MOE2013-T2-1-034; ARC 19/15, no. MOE2014-T2-2-093), AcRF Tier 1 (RG 9/12, RG 61/12, RGT18/ 13, and RG5/13), and Start-Up grant (M4081296.070.500000), A*Star (M4070178.120), and the Singapore-Berkeley Research Initiative for Sustainable Energy (SinBeRISE) for the financial support. This research is also conducted by Nanyang Technological University–Hebrew University of Jerusalem–Ben-Gurion University Nanomaterials for Energy and Water Management Programme under the Campus for Research Excellence and Technological Enterprise, which is supported by the National Research Foundation, Prime Minister's Office, Singapore. Jiazang Chen thanks Dr. Yinghua Xu (Zhejiang University of Technology) and Dr. Tiancheng Xu (HzCell Electrochem. Corp.) for the help on discussion of impedance results.

References and Notes

[1] a) M. Gratzel, *Nature* **2001**, *414*, 338; b) X. Chen, S. S. Mao, *Chem. Rev.* **2007**, *107*, 2891; c) A. Fujishima, K. Honda, *Nature* **1972**, *238*, 37.

[2] a) R. I. Bickley, T. Gonzalez-Carreno, J. S. Lees, L. Palmisano, R. J. D. Tilley, *J. Solid State Chem.* **1991**, *92*, 178; b) Y. K. Kho, A. Iwase, W. Y. Teoh, L. Mädler, A. Kudo, R. Amal, *J. Phys.*

Chem. C **2010**, *114*, 2821; c) T. Ohno, K. Tokieda, S. Higashida, M. Matsumura, *Appl. Catal. A: Gen.* **2003**, *244*, 383.
[3] G. Li, K. A. Gray, *Chem. Phys.* **2007**, *339*, 173.
[4] T. Luttrell, S. Halpegamage, J. G. Tao, A. Kramer, E. Sutter, M. Batzill, *Sci. Rep.* **2014**, *4*, 4043.
[5] a) D. C. Hurum, A. G. Agrios, K. A. Gray, T. Rajh, M. C. Thurnauer, *J. Phys. Chem. B* **2003**, *107*, 4545; b) D. O. Scanlon, C. W. Dunnill, J. Buckeridge, S. A. Shevlin, A. J. Logsdail, S. M. Woodley, C. R. A. Catlow, M. J. Powell, R. G. Palgrave, I. P. Parkin, G. W. Watson, T. W. Keal, P. Sherwood, A. Walsh, A. A. Sokol, *Nat. Mater.* **2013**, *12*, 798; c) L. Kavan, M. Gratzel, S. E. Gilbert, C. Klemenz, H. J. Scheel, *J. Am. Chem. Soc.* **1996**, *118*, 6716.
[6] A. Hagfeldt, G. Boschloo, L. C. Sun, L. Kloo, H. Pettersson, *Chem. Rev.* **2010**, *110*, 6595.
[7] A. J. Frank, N. Kopidakis, J. van de Lagemaat, *Coord. Chem. Rev.* **2004**, *248*, 1165.
[8] a) N. Kopidakis, E. A. Schiff, N. G. Park, J. van de Lagemaat, A. J. Frank, *J. Phys. Chem. B* **2000**, *104*, 3930; b) L. Dloczik, O. Ileperuma, I. Lauermann, L. M. Peter, E. A. Ponomarev, G. Redmond, N. J. Shaw, I. Uhlendorf, *J. Phys. Chem. B* **1997**, *101*, 10281; c) E. Hendry, M. Koeberg, B. O'Regan, M. Bonn, *Nano Lett.* **2006**, *6*, 755; d) J. Villanueva-Cab, S.-R. Jang, A. F. Halverson, K. Zhu, A. J. Frank, *Nano Lett.* **2014**, *14*, 2305; e) J. E. Kroeze, T. J. Savenije, J. M. Warman, *J. Am. Chem. Soc.* **2004**, *126*, 7608; f) K. Zhu, N. R. Neale, A. Miedaner, A. J. Frank, *Nano Lett.* **2007**, *7*, 69.
[9] a) E. Palomares, J. N. Clifford, S. A. Haque, T. Lutz, J. R. Durrant, *J. Am. Chem. Soc.* **2003**, *125*, 475; b) J. R. Durrant, S. A. Haque, E. Palomares, *Coord. Chem. Rev.* **2004**, *248*, 1247.
[10] a) J. van de Lagemaat, K. D. Benkstein, A. J. Frank, *J. Phys. Chem. B* **2001**, *105*, 12433; b) J. Chen, H. B. Yang, J. Miao, H.-Y. Wang, B. Liu, *J. Am. Chem. Soc.* **2014**, *136*, 15310.
[11] a) J. Livage, M. Henry, C. Sanchez, *Prog. Solid State Chem.* **1988**, *18*, 259; b) M. Henry, J. Jolivet, J. Livage, in *Chemistry, Spectroscopy and Applications of Sol-Gel Glasses*, Vol. 77 (Eds: R. Reisfeld, C. K. Jjørgensen), Springer Berlin Heidelberg, **1992**, 153.
[12] F. Fabregat-Santiago, J. Bisquert, G. Garcia-Belmonte, G. Boschloo, A. Hagfeldt, *Sol. Energy Mater. Sol. Cells* **2005**, *87*, 117.
[13] a) J. Bisquert, *J. Phys. Chem. B* **2001**, *106*, 325; b) F. Fabregat-Santiago, G. Garcia-Belmonte, J. Bisquert, A. Zaban, P. Salvador, *J. Phys. Chem. B* **2002**, *106*, 334; c) F. Fabregat-Santiago, J. Bisquert, E. Palomares, L. Otero, D. B. Kuang, S. M. Zakeeruddin, M. Gratzel, *J. Phys. Chem. C* **2007**, *111*, 6550.
[14] J. Bisquert, *Phys. Chem. Chem. Phys.* **2008**, *10*, 49.
[15] I. Abayev, A. Zaban, F. Fabregat-Santiago, J. Bisquert, Vol. 196, WILEY-VCH Verlag, **2003**, R4.
[16] F. Fabregat-Santiago, J. Bisquert, L. Cevey, P. Chen, M. K. Wang, S. M. Zakeeruddin, M. Gratzel, *J. Am. Chem. Soc.* **2009**, *131*, 558.
[17] J. Bisquert, V. S. Vikhrenko, *J. Phys. Chem. B* **2004**, *108*, 2313.
[18] V. Pfeifer, P. Erhart, S. Li, K. Rachut, J. Morasch, J. Brötz, P. Reckers, T. Mayer, S. Rühle, A. Zaban, I. Mora Seró, J. Bisquert, W. Jaegermann, A. Klein, *J. Phys. Chem. Lett.* **2013**, *4*, 4182.
[19] a) T. Tiedje, J. M. Cebulka, D. L. Morel, B. Abeles, *Phys. Rev. Lett.* **1981**, *46*, 1425; b) J. Orenstein, M. Kastner, *Phys. Rev. Lett.* **1981**, *46*, 1421.
[20] a) A. Hagfeldt, M. Graetzel, *Chem. Rev.* **1995**, *95*, 49; b) J. van de Lagemaat, A. J. Frank, *J. Phys. Chem. B* **2000**, *104*, 4292; c) D. Cahen, G. Hodes, M. Gratzel, J. F. Guillemoles, I. Riess, *J. Phys. Chem. B* **2000**, *104*, 2053.
[21] N. Kopidakis, N. R. Neale, A. J. Frank, *J. Phys. Chem. B* **2006**, *110*, 12485.
[22] a) H. Tang, K. Prasad, R. Sanjinès, P. E. Schmid, F. Lévy, *J. Appl. Phys.* **1994**, *75*, 2042; b) L.

Forro, O. Chauvet, D. Emin, L. Zuppiroli, H. Berger, F. Lévy, *J. Appl. Phys.* **1994**, *75*, 633.
[23] S. Ito, P. Liska, P. Comte, R. Charvet, P. Pechy, U. Bach, L. Schmidt-Mende, S. M. Zakeeruddin, A. Kay, M. K. Nazeeruddin, M. Gratzel, *Chem. Commun.* **2005**, 4351.
[24] S. Nakade, T. Kanzaki, Y. Wada, S. Yanagida, *Langmuir* **2005**, *21*, 10803.
[25] A. Zaban, M. Greenshtein, J. Bisquert, *ChemPhysChem* **2003**, *4*, 859.

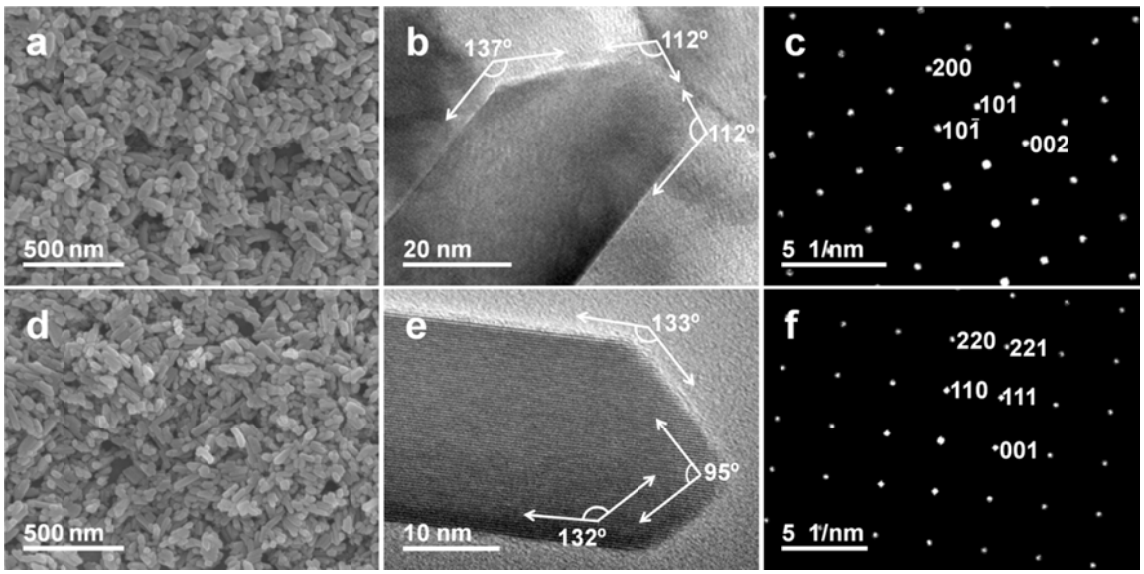

Figure 1. Characteristics of the TiO_2 nanostructures. a) FESEM image, b) TEM image, and c) SAED pattern of the anatase TiO_2 nanorods synthesized by hydrothermal treatment of titanium isopropoxide in alcoholic ammonia water system. d) FESEM image, e) TEM image, and f) SAED pattern for the rutile TiO_2 nanorods obtained by hydrothermal treatment of $TiCl_4$ (final concentration of 0.5 M in the reaction autoclave). It can be seen that the size (a, d) and shape (b, e) of these two polymorphs of TiO_2 are very similar.

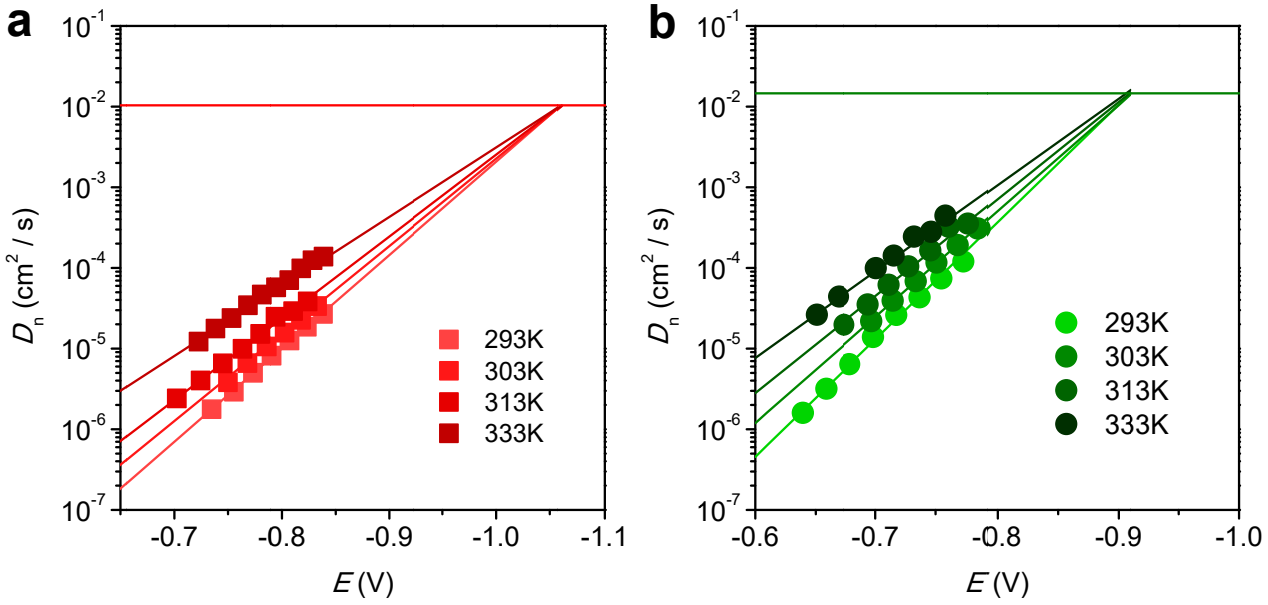

Figure 2. Temperature-dependent diffusion coefficient of electrons in TiO_2 electrodes. Electron diffusion coefficient for a) rutile and b) anatase TiO_2 electrodes over the measured potential range under various temperatures. The trap-free diffusion coefficient (D_0) of electrons in the electrodes can be obtained by extrapolating the D_n plots. The D_0 values for rutile and anatase TiO_2 electrodes are 0.0104 and 0.0147 cm^2/s, respectively, corresponding to 0.402 and 0.568 cm^2/Vs for electron mobility. Parameters, such as electronic conductivity, chemical capacitance, and diffusion coefficient D_n in the electrodes, were obtained by fitting and calculating the data from the impedance spectra.

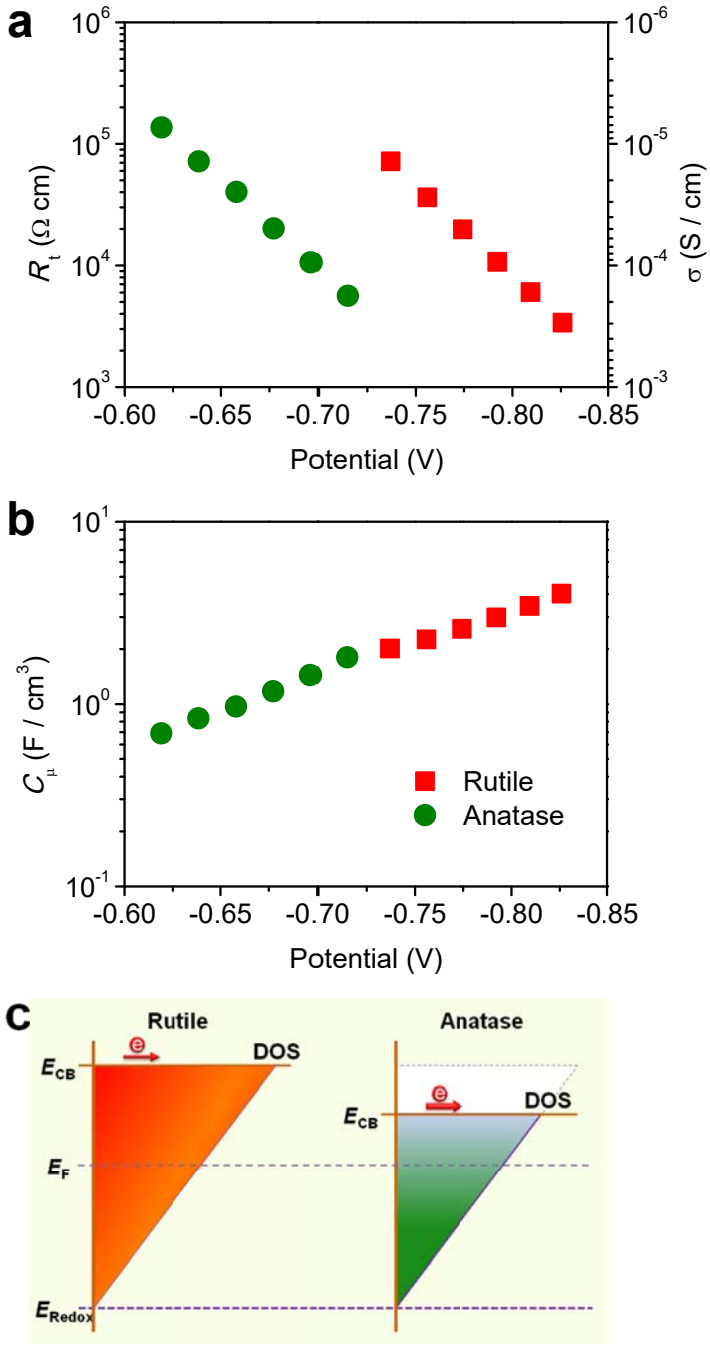

Figure 3. Density and distribution of electronic states in the semiconductor electrodes. a) Charge transport resistance and electronic conductivity and, b) chemical capacitance of rutile and anatase TiO_2-based mesoporous electrodes varied along the electrode potentials. c) Schematic illustration for the energetics, and density and distribution of trap states in the TiO_2 electrodes. Although the mobility of electrons in the rutile electrode is slightly lower than that in the anatase one (Figure 2), the difference in their conductivity is more obvious. Therefore, it is safe to conclude that the conduction band edge of rutile is higher than that of anatase (c).

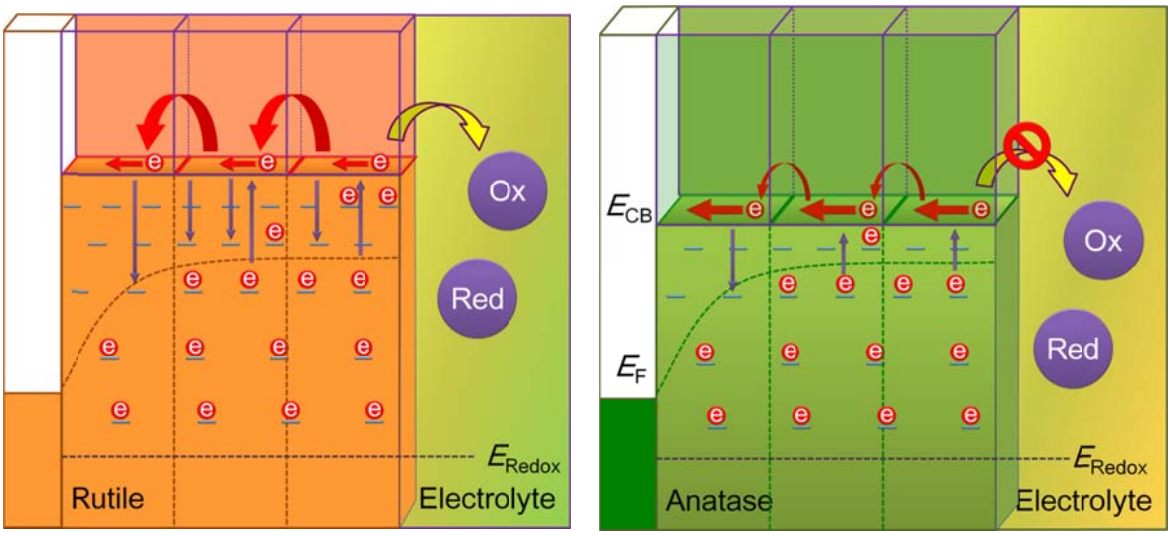

Figure 4. Schematic illustration of the features of electronic processes occurring in rutile (left) and anatase (right) TiO_2-based photoelectrochemical cells. As illustrated in the schemes, the trap-free diffusion of electrons in the conduction band consists of two parts, i.e. the internal electron movement and inter-grain charge transfer, which are connected in series. Although the internal electron movement in anatase TiO_2 is faster than that in rutile polymorph, the inter-grain charge transfer is not as efficient as that in rutile TiO_2. As a result, the D_0 values for these two electrodes are very similar (Figure 2). Despite of the similar D_0 value, the higher density of trap sites in the band gap of the rutile electrode increases the probability of trapping/detrapping events during the charge transport, resulting in lowering of charge diffusion coefficient (Figure S7). Moreover, the higher density of trap states in the rutile electrode will aggravate the interfacial charge recombination (Figure S8). The straight arrows represent the internal electron movement inside the building blocks, while the curved arrows show the inter-grain charge transfer during the charge transport procedures.

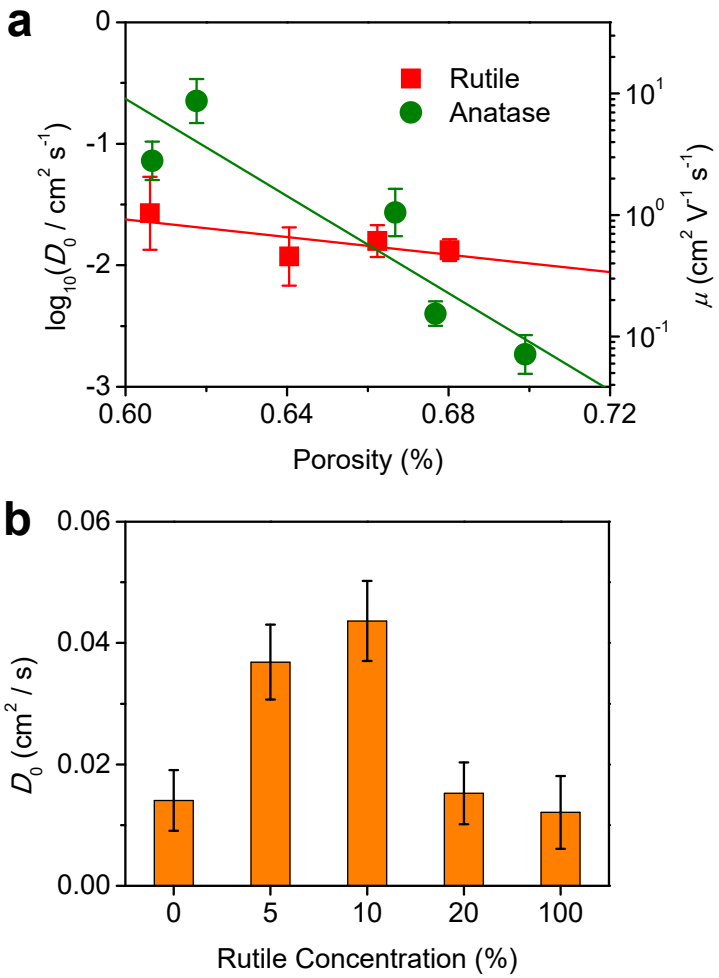

Figure 5. Porosity and intergradient dependent trap-free diffusion coefficient of electrons in the porous semiconductor electrodes. a) Trap-free diffusion coefficient of electrons in rutile and anatase TiO_2-based electrodes with various porosities. b) Trap-free diffusion coefficient of electrons in TiO_2 electrodes composed of mixed phases of rutile and anatase.

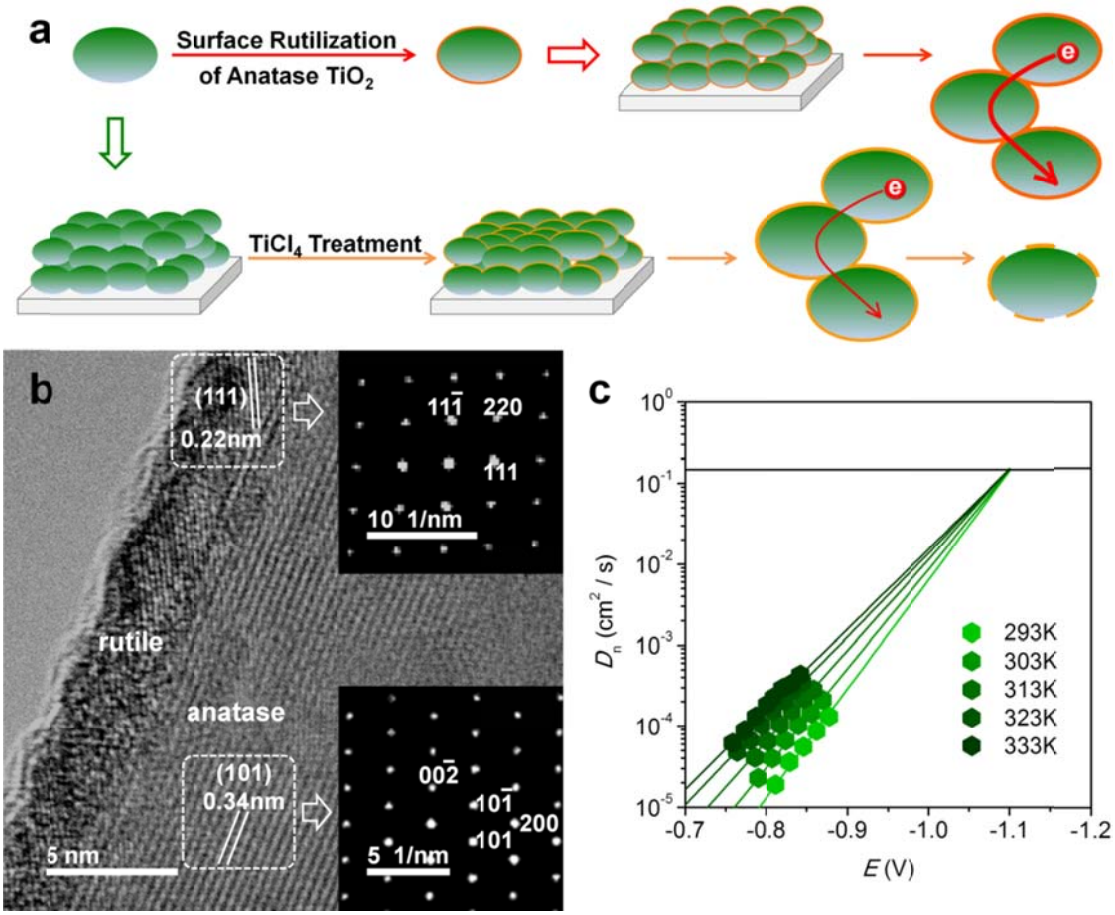

Figure 6. Features of semiconductor electrodes based on surface rutilized anatase nanostructures. a) Schematic illustration of the fabrication of TiO_2 electrodes using surface rutilized anatase nanostructures (upper). For comparison, the common technique used for $TiCl_4$ treatment of TiO_2 electrode is also presented (bottom). It can be seen that the inter-grain connectivity between adjacent building blocks is rather different for electrodes fabricated by these two routes. For the electrodes using surface rutilized TiO_2 (upper), the adjacent anatase building blocks are intermediated by the thin rutilized layer. For the $TiCl_4$ treated electrodes (bottom), the treatment just modifies the exposed surface; while the inter-grain connectivity remains unchanged. By extracting the individual building block from the $TiCl_4$ treated electrode, it can be seen that the particles are only partially and loosely coated by the formed TiO_2 layers (bottom), which is quite different from the situation of fully coated rutilized layers in our system (upper). b) HRTEM image showing the formation of rutilized thin layer on the surface of anatase TiO_2 nanorods. Insets show the SAED patterns taken on the surface (upper) and bulk (bottom) of the TiO_2 nanostructures. The surface coating layer looks different from the bulk crystal, suggesting the phase transformation occurring on the surface of the TiO_2 nanostructures (the change and transformation of the surface features are specifically shown in Figure S13). The SAED pattern (upper, inset) obtained on the surface of the nanostructures matches well with the reciprocal lattice of rutile along the [1-10] zone axis. The lattice fringes on the surface of the nanostructures are also very close to the (111) interplanar spacing of rutile TiO_2. Besides, XRD patterns (Figure S13) further confirm that the newly formed phase is of rutile TiO_2. c) Temperature-dependent diffusion coefficients of electrons in the electrodes composed of surface rutilized anatase TiO_2 nanostructures. The trap-free diffusion coefficient of electrons in this type of electrodes reaches as high as 0.148 cm^2/s, which is most likely resulted from the excellent electronic connectivity between adjacent building blocks, provides the efficient inter-grain charge transfer for transport of charges in the porous electrodes.

TOC

Transport of charges in the TiO_2 electrodes can be improved by bridging and fencing the electronic highways, which can be realized by surface rutilization of the anatase building blocks prior to fabrication of the electrodes. The ultrathin rutilized phase can promote the inter-grain electronic-connectivity and facilitate charge transfer between adjacent building blocks while suppress the charge recombination on semiconductor-electrolyte interface.

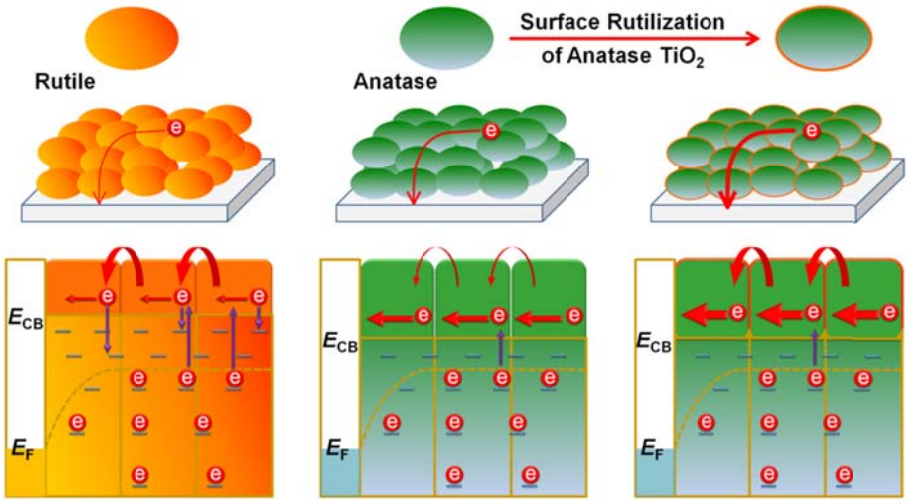

Supporting Information

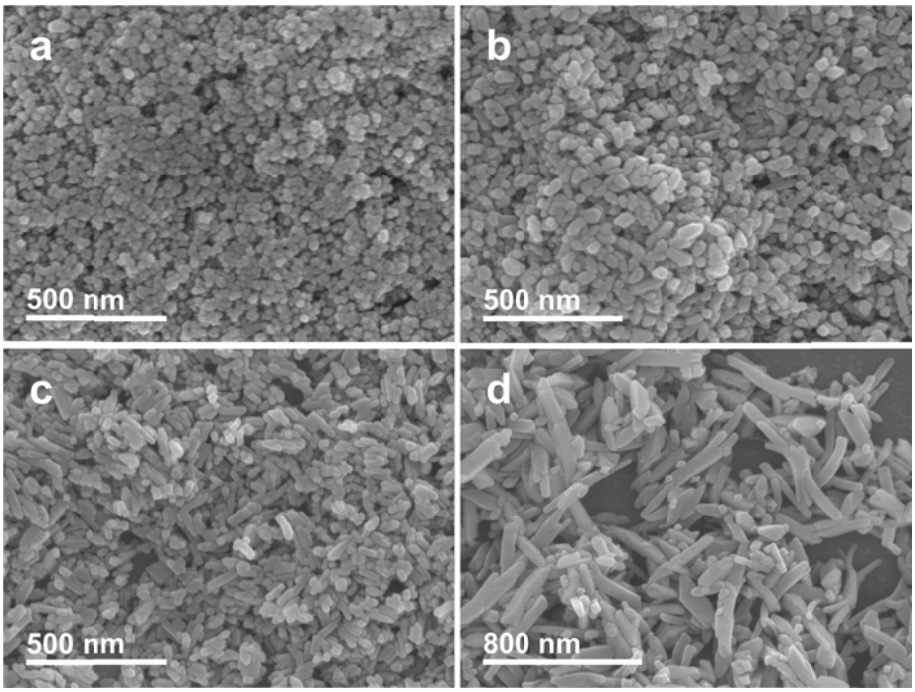

Figure S1. Effect of concentration of ammonia solution on the morphologies of anatase TiO_2 nanostructures. The products were obtained by hydrothermal treatment of titanium isopropoxide in the presence of ammonia water with various concentrations. The volume ratio of ammonia water (28-30%) to the diluting water in reaction is: a) 0: 1, b) 1: 4, c) 2: 3, and d) 1: 0. It can be seen from the FESEM images that as the concentration of ammonia increases, all morphological features including the aspect ratio, length, and diameter of the nanostructures become larger.

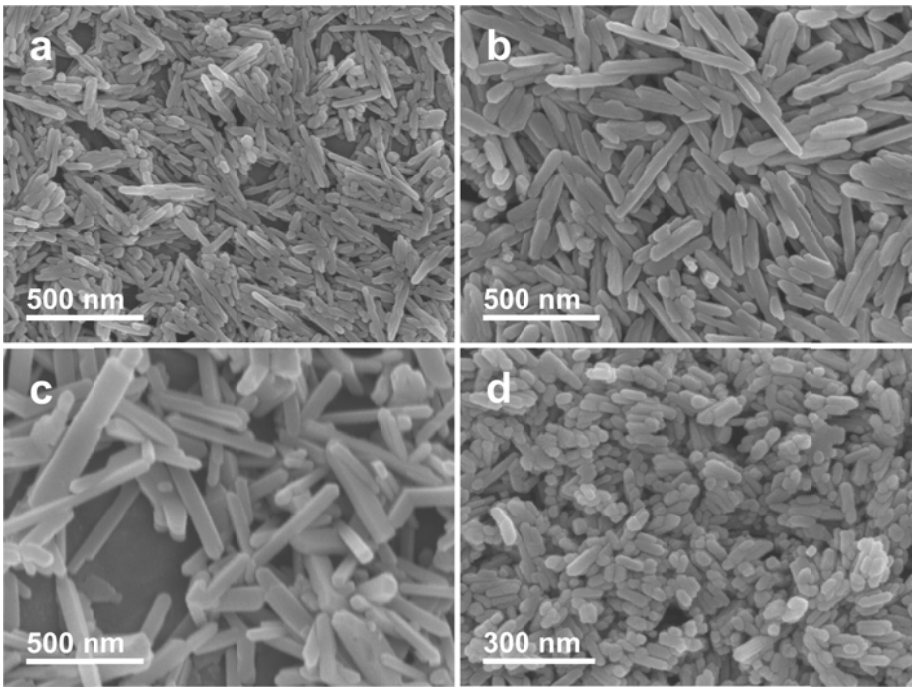

Figure S2. Effect of HCl concentration and titanium precursor on the morphology of rutile TiO_2 nanostructures. a-c) FESEM images of the rutile TiO_2 nanorods prepared by hydrothermal treatment of titanium butoxide (1 mL) in HCl (30 mL) solution at 160 ºC for 12 h. The concentrations of HCl are a) 4 M, b) 6 M, and c) 9 M. d) FESEM images of the rutile TiO_2 nanorods prepared by hydrothermal treatment of titanium tetrachloride. From the FESEM images (a-c), it can be seen that as the concentration of HCl increases, the diameter of rutile nanorods increases, while the aspect ratio decreases. By replacing titanium butoxide with titanium tetrachloride, the diameter and aspect ratio decrease, most likely due to the retardation of hydrolysis and the suppression of linear assembly of the monomers by sharing opposite edges in the equatorial of octahedrons.

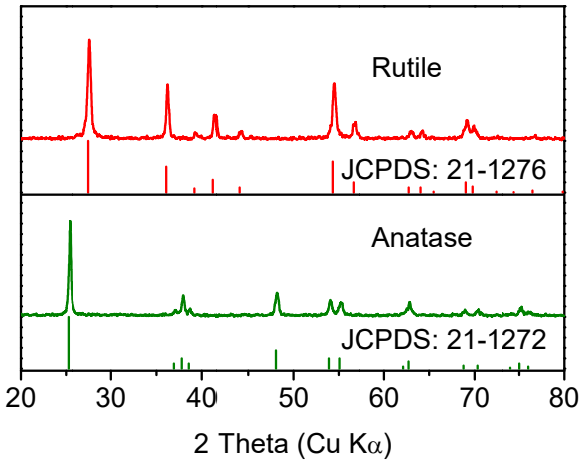

Figure S3. XRD patterns for the TiO_2 nanostructures grown in acidic and alcoholic ammonia water systems. It can be seen from the XRD patterns that the TiO_2 nanostructure obtained by hydrothermal treatment of $TiCl_4$ (upper, red) is crystalline rutile phase, while the product prepared from titanium isopropoxide precursor in alcoholic ammonia water systems (bottom, olive) is anatase phase.

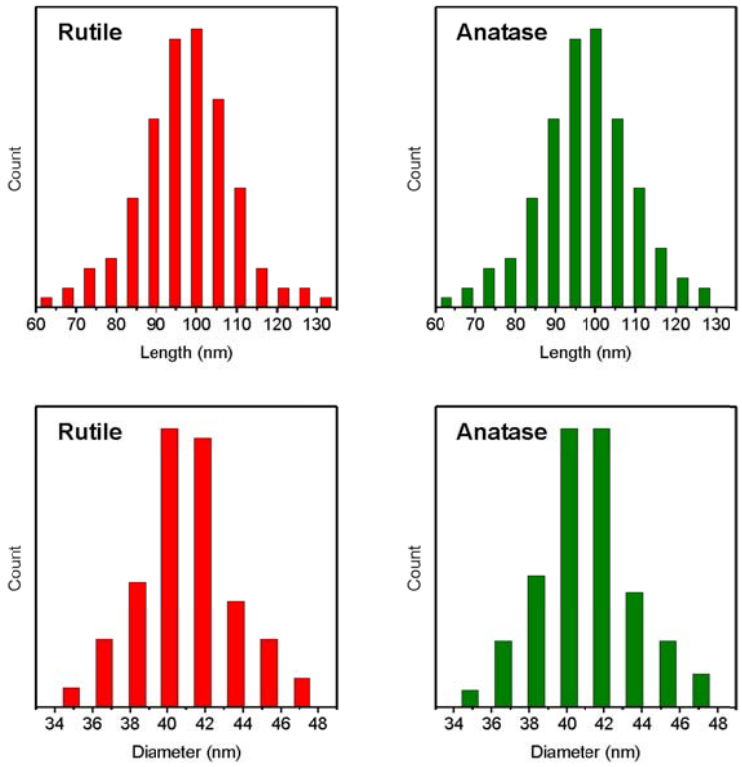

Figure S4. Diameter and length distribution of the rutile and anatase TiO_2 nanostructures. It can be seen that the size for each polymorph of the TiO_2 nanorods is very similar.

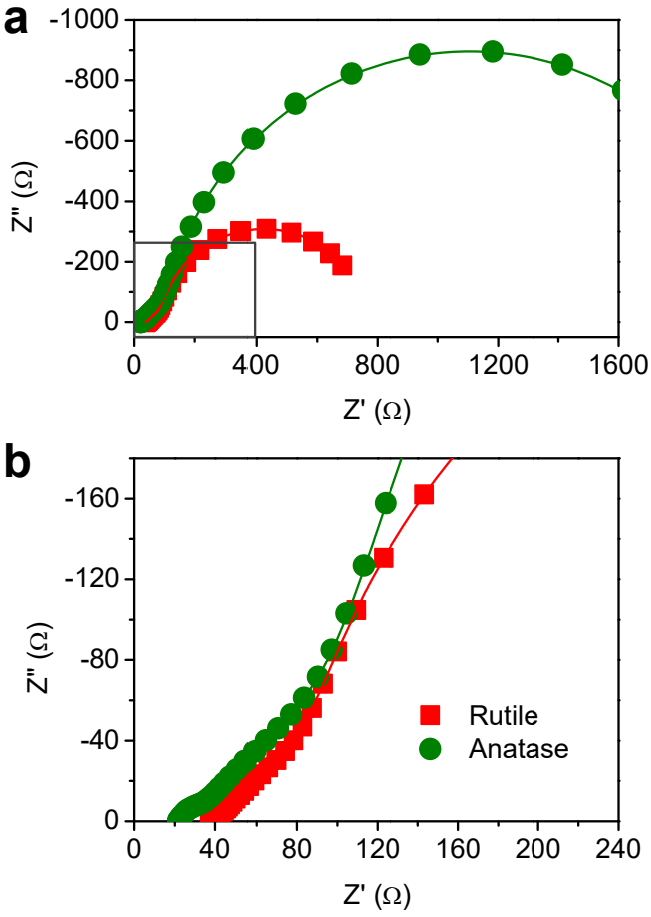

Figure S5. Electrochemical impedance spectra of the cells. a) Nyquist plots of the impedance spectra of the cells measured at the bias of -0.74 V (rutile) and -0.68 V (anatase). b) Magnification

of the high-frequency region in the plot in (a).

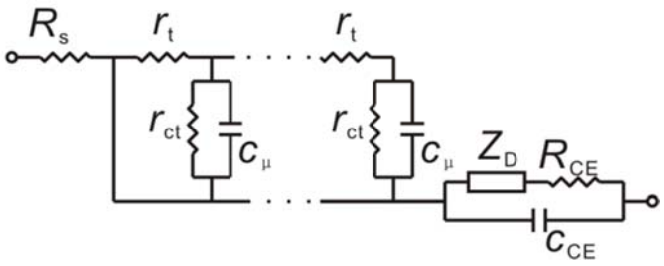

Figure S6. Transmission line model used for fitting the impedance spectra. r_{ct} is the resistance for the charge recombination process between electrons and I_3^- in the electrolyte; c_μ is the chemical capacitance of TiO_2 film; R_{CE} and C_{CE} are the charge transfer resistance and double-layer capacitance at the counter electrode (platinized TCO glass), respectively; and R_S is the series resistance, including the sheet resistance of TCO glass and the contact resistance of the cell.

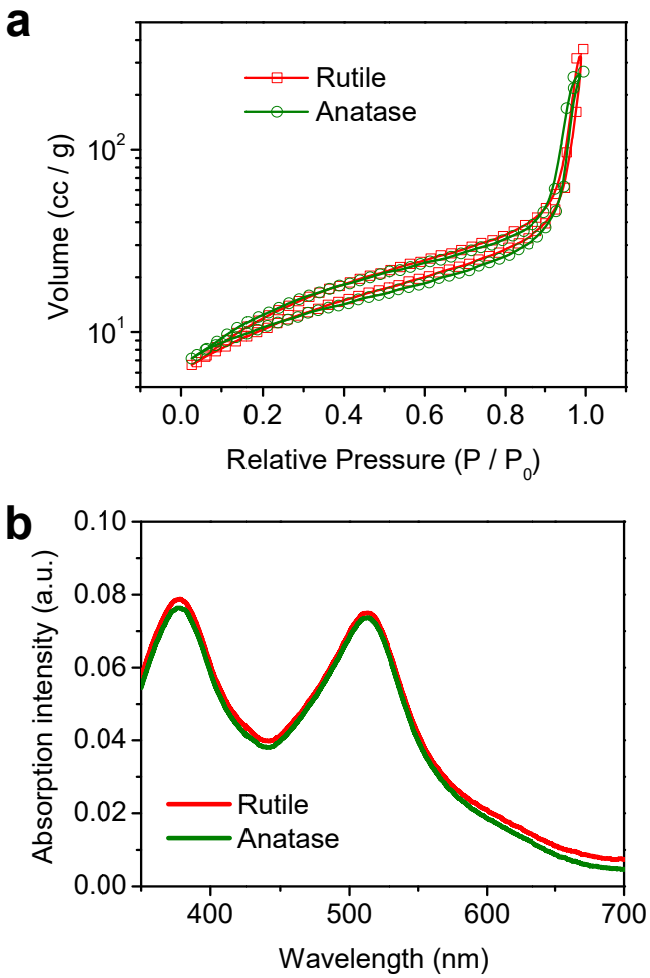

Figure S7. Architectural characterizations of the TiO_2 electrodes. a) Nitrogen adsorption-desorption isotherm of rutile and anatase electrodes. b) UV-Vis absorption spectra of the N719 dye desorbed from the sensitized electrodes. The amounts of dye desorbed from the electrodes are 5.71×10^{-8} and 5.63×10^{-8} mol/cm^2 for rutile and anatase TiO_2 electrodes, corresponding to 4.79×10^{-8} and 4.77×10^{-5} mol/cm^3 with respect to film volume, respectively. From (a) and (b), it can be seen that the constructions of electrodes made of rutile and anatase nanostructures are very similar.

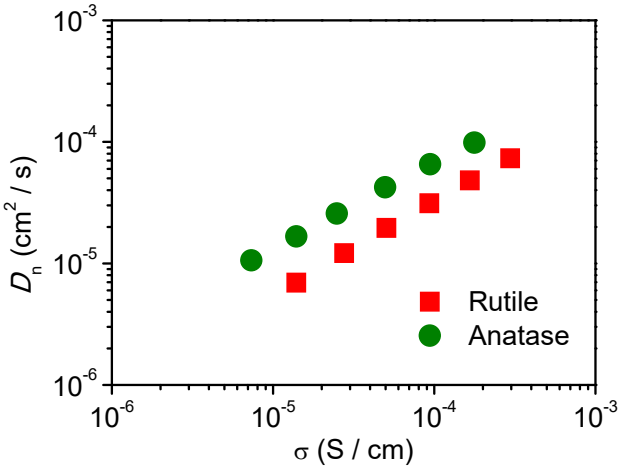

Figure S8. Diffusion coefficient of electrons in rutile and anatase TiO_2-based mesoporous electrodes as a function of electronic conductivity. Due to the high probability of trapping/detrapping events during the electron transport procedures, the charge diffusion coefficient for the rutile electrode is lower than that of anatase electrode.

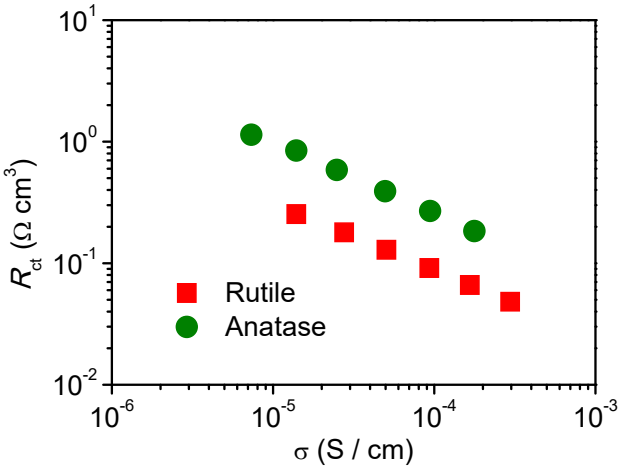

Figure S9. Features of interfacial charge transfer in the electrodes made of rutile and anatase TiO_2 nanostructures. Variation of interfacial charge recombination resistance over the measured conductivity range.

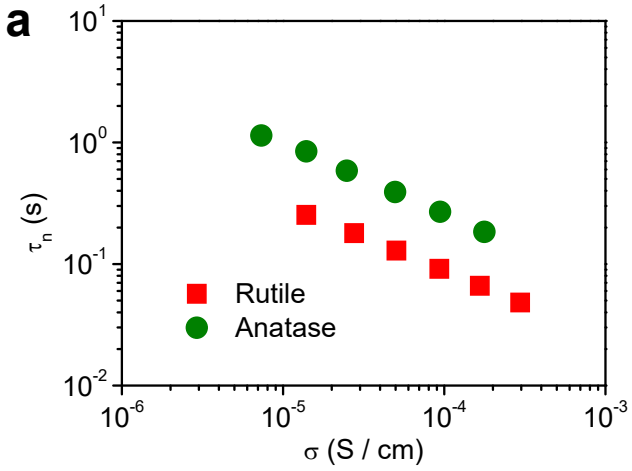

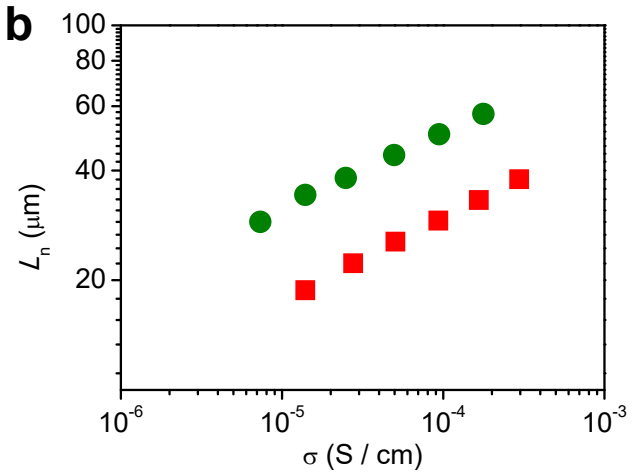

Figure S10. Effect of trap states on the electronic processes occurred in the TiO_2 electrodes. a) Lifetime and b) diffusion length of electrons in rutile and anatase TiO_2-based mesoporous electrodes varied with the change of electronic conductivity.

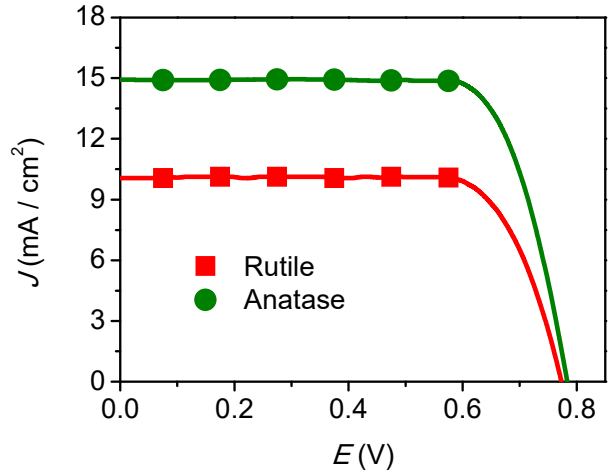

Figure S11. Photocurrent-voltage characteristics of the dye-sensitized nanostructured TiO_2-based photovoltaic devices. The detailed photovoltaic parameters, including open-circuit voltage (V_{OC}), short-circuit photocurrent density (J_{SC}), fill factor (FF), and overall energy conversion efficiency (η) are 773 mV, 10.06 mA/cm^2, 0.760, and 5.91 % for the rutile cell and 783 mV, 14.93 mA/cm^2, 0.763, and 8.92 % for the anatase cell, respectively.

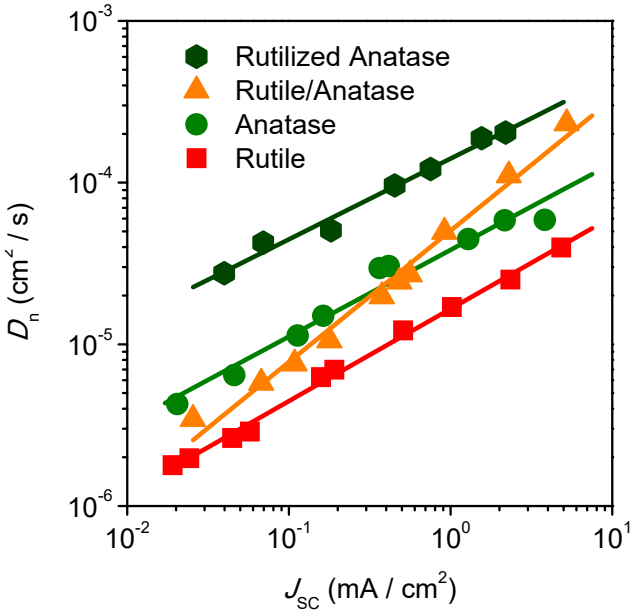

Figure S12. Relationship between charge diffusion coefficient and illumination intensity for the cells composed of different TiO_2 electrodes. The plots for electron diffusion coefficients over various short-circuit photocurrent densities were obtained by stepped light-induced photocurrent transient measurement under various illumination intensities.

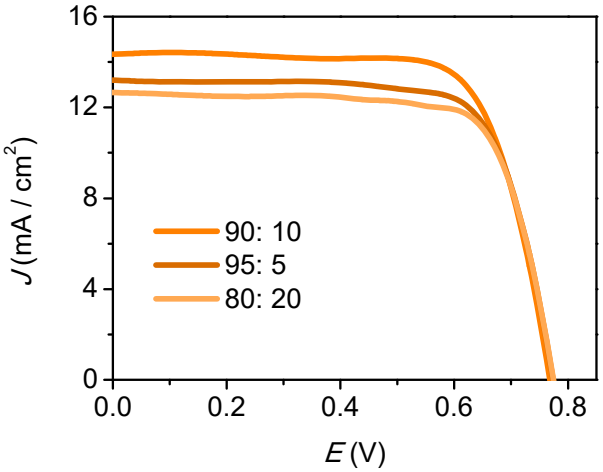

Figure S13. Photocurrent-voltage characteristics of the photovoltaic device based on mixed phase TiO_2. Although the trap-free diffusion coefficient of electrons in mixed phase TiO_2 electrode reaches as high as 0.0436 cm^2/s (Figure 5b), the relatively high density of trap states as introduced by addition of the rutile TiO_2 increases the probability of trapping/detrapping events, especially in the case of low density of charge carriers. As a result, the photovoltaic performance of the cell with phase-mixed TiO_2 electrode shows even poorer performance compared to the pure anatase TiO_2 electrode. The photovoltaic device with phase-mixed TiO_2 (90 wt% of anatase and 10 wt% of rutile) gives the energy conversion of 8.16%, with the photovoltaic parameters of 769 mV, 14.34 mA/cm^2, and 0.740 for the open-circuit voltage, short-circuit photocurrent density, and fill factor, respectively. For the other two photovoltaic devices based on composite electrodes, the energy conversions are slightly lower. The detailed photovoltaic parameters, including open-circuit voltage, short-circuit photocurrent density, fill factor, and overall energy conversion efficiency for each cell are 772 mV, 13.21 mA/cm^2, 0.749, and 7.59 % (95 wt% of anatase and 5 wt% of rutile) and 775 mV, 12.66 mA/cm^2, 0.752, and 7.38 % (80 wt% of anatase and 20 wt% of rutile), respectively.

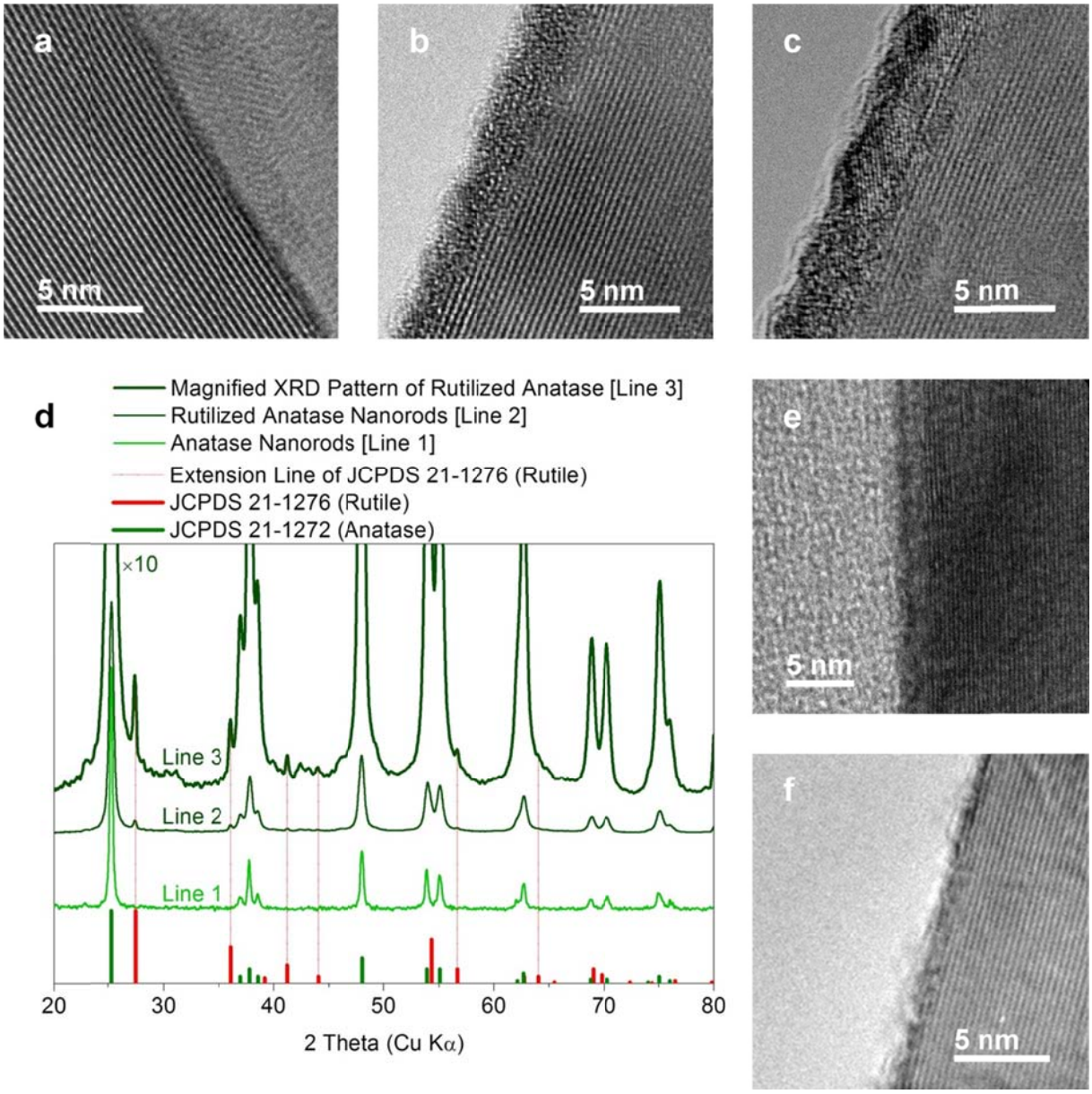

Figure S14. Features of surface rutilized anatase TiO_2 nanostructures. a-c) TEM images for the anatase TiO_2 nanostructures before (a) and after (b, c) surface rutilization. By comparing these TEM images, it can be seen that the anatase lattice in the surface obviously changed and transformed to other crystalline phase (comparing a and c), while the bulk crystal remained unchanged (comparing a and b). The TEM images shown in (b) and (c) are taken from the same nanostructures, while the focal distances are tuned to show the crystalline lattice in the bulk (b) and on the surface (c). d) XRD patterns for the anatase TiO_2 nanostructures before (Line 1) and after (Line 2 and Line 3) surface rutilization. The appearance of rutile phase further confirms that the surface of anatase TiO_2 nanostructures is rutilized. e, f) TEM images for the surface rutilized nanostructures obtained by the hydrothermal treatment of anatase TiO_2 nanostructures in HCl solution at reaction temperature of 180 ºC for 72 h (e) and reaction temperature of 200 ºC for 24 h (f). It can be seen that the crystallinity in (e) is lower and the thickness in (f) of the rutilized layers becomes smaller, as compared with the case obtained from the reaction at 200 ºC for 72 h (b, c).

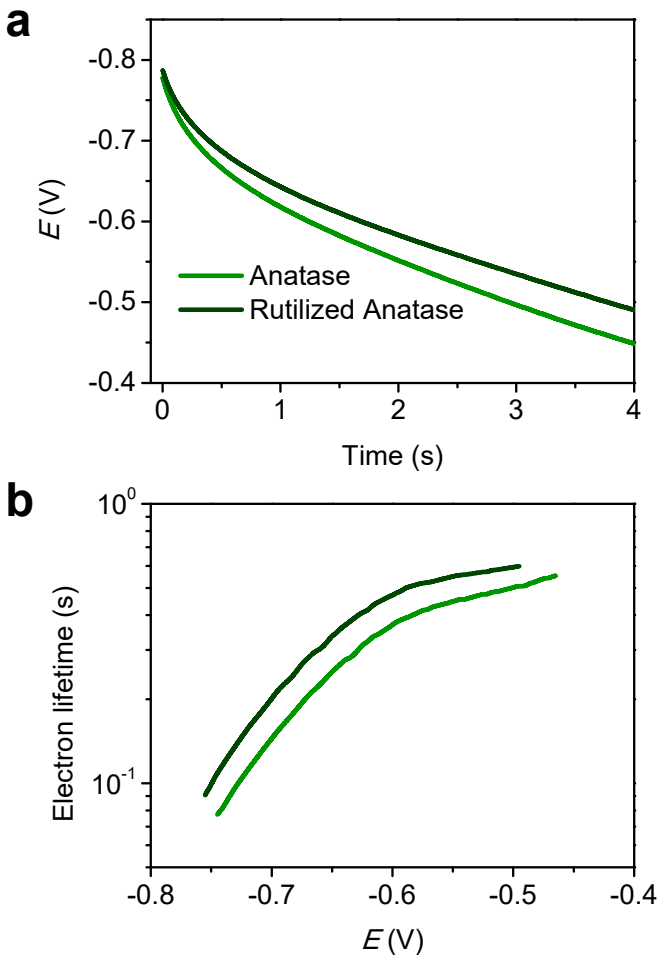

Figure S15. Retarding of interfacial charge recombination by the rutilized surface. a) Open-circuit voltage decay (OCVD) spectra of the cells with phase-pure anatase and surface rutilized anatase TiO_2 nanostructure electrodes. b) Electron lifetime derived from the OCVD spectra. It can be seen that the electrodes made of surface rutilized anatase TiO_2 nanostructures can effectively protect the electrons from recombination at the semiconductor-electrolyte interface by blocking the interfacial charge transfer, due to the slightly higher position of the conduction band of rutilized layer.

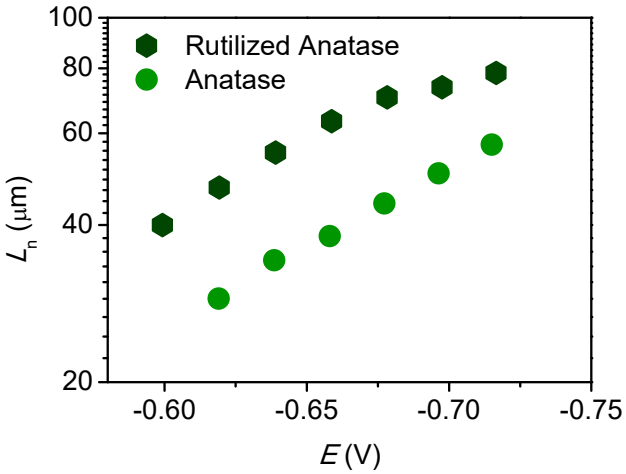

Figure S16. Effect of surface rutilized layer on the collection of charges in TiO_2 electrodes. Diffusion length of electrons in the electrodes made of pure anatase TiO_2 and surface rutilized anatase TiO_2 nanostructures.

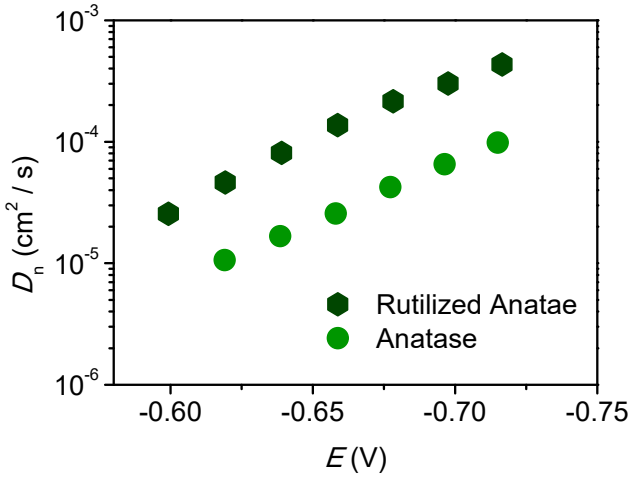

Figure S17. Plots of diffusion coefficient of electrons in the electrodes made of phase-pure and surface rutilized anatase TiO_2 nanostructures as function of potentials. It can be seen that the surface rutilized layers can significantly improve the diffusion of charges in the TiO_2 electrodes.

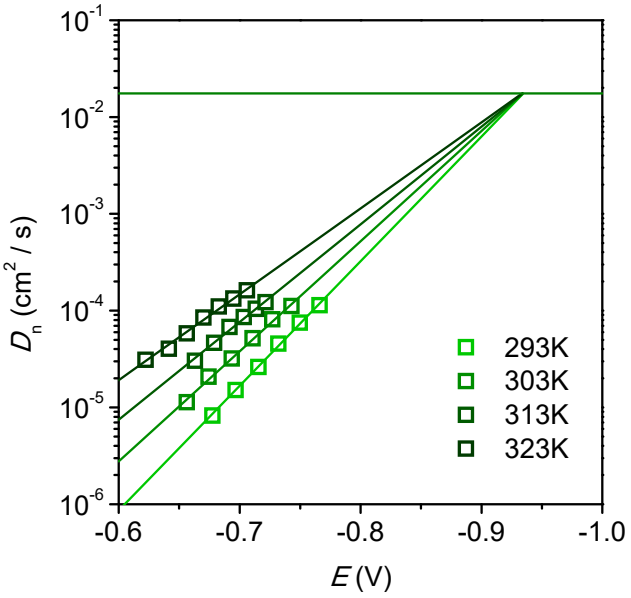

Figure S18. Temperature-dependent diffusion coefficients of electrons in the $TiCl_4$ post-treated anatase TiO_2 electrodes. Since the $TiCl_4$ treatment did not form the bridging rutile thin layer between the adjacent anatase building blocks, the effect on the charge transport is very tiny. The trap-free diffusion coefficient (D_0) of electrons in this type of electrode is 0.0175 cm^2/s, which is very similar with the untreated electrode (0.0147 cm^2/s, Figure 2).

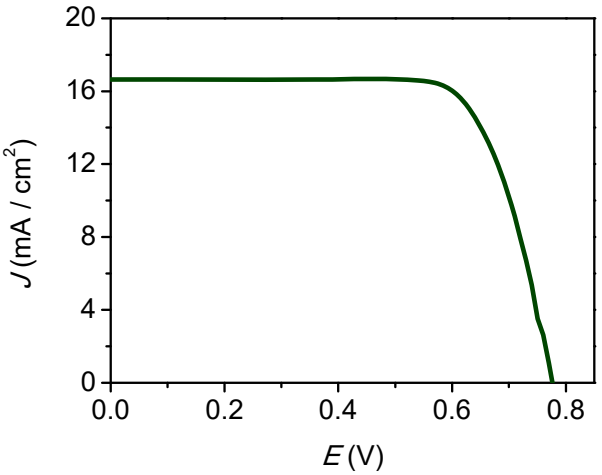

Figure S19. Photocurrent-voltage characteristics of the photovoltaic device based on surface rutilized anatase TiO_2 nanostructures. The obtained open-circuit voltage (V_{OC}), short-circuit photocurrent density (J_{SC}), fill factor (*FF*), and overall energy conversion efficiency (η) are 776 mV, 16.65 mA/cm^2, 0.745, and 9.62%, respectively.